Targeting cancer cell integrins using gold nanorods in photothermal therapy inhibits migration through affecting cytoskeletal proteins

Moustafa R. K. Ali[a,1], Yue Wu[a,1], Yan Tang[b], Haopeng Xiao[a], Kuangcai Chen[c], Tiegang Han[a], Ning Fang[c,2], Ronghu Wu[a,2], and Mostafa A. El-Sayed[a,d,2]

[a]School of Chemistry and Biochemistry, Georgia Institute of Technology, Atlanta, GA 30332; [b]School of Chemical and Bimolecular Engineering, Georgia Institute of Technology, Atlanta, GA 30332; [c]Department of Chemistry, Georgia State University, Atlanta, GA 30302; and [d]School of Chemistry, King Abdul Aziz University, Jeddah 23218, Saudi Arabia

Contributed by Mostafa A. El-Sayed, May 18, 2017 (sent for review February 24, 2017; reviewed by Bjoern M. Reinhard and Weihong Tan)

Metastasis is responsible for most cancer-related deaths, but the current clinical treatments are not effective. Recently, gold nanoparticles (AuNPs) were discovered to inhibit cancer cell migration and prevent metastasis. Rationally designed AuNPs could greatly benefit their antimigration property, but the molecular mechanisms need to be explored. Cytoskeletons are cell structural proteins that closely relate to migration, and surface receptor integrins play critical roles in controlling the organization of cytoskeletons. Herein, we developed a strategy to inhibit cancer cell migration by targeting integrins, using Arg–Gly–Asp (RGD) peptide-functionalized gold nanorods. To enhance the effect, AuNRs were further activated with 808-nm near-infrared (NIR) light to generate heat for photothermal therapy (PPTT), where the temperature was adjusted not to affect the cell viability/proliferation. Our results demonstrate changes in cell morphology, observed as cytoskeleton protrusions—*i.e.*, lamellipodia and filopodia—were reduced after treatment. The Western blot analysis indicates the downstream effectors of integrin were attracted toward the antimigration direction. Proteomics results indicated broad perturbations in four signaling pathways, Rho GTPases, actin, microtubule, and kinases-related pathways, which are the downstream regulators of integrins. Due to the dominant role of integrins in controlling cytoskeleton, focal adhesion, actomyosin contraction, and actin and microtubule assembly have been disrupted by targeting integrins. PPTT further enhanced the remodeling of cytoskeletal proteins and decreased migration. In summary, the ability of targeting AuNRs to cancer cell integrins and the introduction of PPTT stimulated broad regulation on the cytoskeleton, which provides the evidence for a potential medical application for controlling cancer metastasis.

gold nanorods | cytoskeleton | integrin | metastasis | plasmonic photothermal therapy

Metastasis is a process that enables cancer cells to spread to other sites of the body and is responsible for most cancer-related deaths (1–3). The migration of cancer cells from one site to another requires dramatic remodeling of the cellular cytoskeleton (2–5). Studies on the changes of cytoskeletal components could provide novel therapeutic approaches to prevent cancer cell migration and metastasis (4). The targeting of cytoskeletal components, such as actin or tubulin (6, 7), or regulatory proteins, such as Rho-ROCK or LIM kinases, has been shown to inhibit the invasive and metastatic behavior of cancer cells (8, 9). However, the pharmacological inhibitors of cytoskeleton have not been very effective in clinical trials due to their nonspecific targeting of cytoskeleton in normal cells, which might cause side effects, such as cardiotoxicity (4, 7, 10). Moreover, in many cases, the anticancer drugs that target specific proteins might lose their efficacy after several months of treatment due to mutations of the proteins that result in the rise of drug resistance in cancer cells (11, 12).

Recent advancements in nanomedicine provide us with great opportunities to avoid the drawbacks of commonly used drugs (13, 14). Due to their small size and surface modifications, nanoparticles, in general, are able to target tumors selectively (15) and have been widely used in cancer diagnosis and therapy (16, 17). The recent discovery of nanoparticles' effect on inhibiting cancer cell migration or metastasis starts to draw the attention of researchers (18–22). However, high concentrations of nontargeted nanoparticles (in μM) were used in these previous studies, which might be an obstacle when considering the translation to clinical use. Additionally, several types of nanoparticles, including TiO_2, SiO_2, iron oxide, etc., have been found to exhibit toxicity when used in relatively high concentrations (23–25). In our previous work, we designed nuclear membrane-targeted gold nanoparticles (AuNPs) for inhibiting cancer cell migration by increasing their nuclear stiffness, which greatly reduced AuNP dosage and could be favorable for clinical applications (26). Therefore, to maintain the nanoparticles' effect on impeding cancer cell migration, an intelligent design with a reduced quantity of nanoparticles promises to be crucial in the development of novel and effective antimetastasis therapy. In addition, the preliminary observations of several groups have shown that this inhibition effect of nanoparticles is related to some individual cytoskeleton proteins (18, 19, 22), such as microtubule and actin. However, various mechanisms have been proposed. Tay et al. (18) found that TiO_2, SiO_2, and hydroxyapatite nanoparticles could slow cancer cell migration by disrupting the intracellular microtubule assembly. Soenen et al. (19) reported that iron oxide nanoparticles at high concentrations within cells affect the cellular cytoskeleton and focal adhesion kinase. Zhou et al. (22) showed gold nanorods (AuNRs) can inhibit ATP production and thus inhibit F-actin cytoskeletal assembly and decrease

Significance

Metastasis is the primary cause of cancer-related deaths. Current clinical treatments for antimetastasis, however, are not effective. This work aims to develop a strategy to inhibit cancer cell migration using gold nanorods (AuNRs) with systematic understanding of the mechanism. The ability of targeting AuNRs to cancer cell surface integrins and the introduction of NIR light to generate a mild plasmonic photothermal effect caused broad regulation on cytoskeletal proteins, thus impairing cancer cell migration. This strategy provides a potential application for controlling cancer metastasis.

Author contributions: M.R.K.A., Y.W., and M.A.E.-S. designed research; M.R.K.A., Y.W., H.X., and K.C. performed research; M.R.K.A., Y.W., H.X., K.C., N.F., and R.W. contributed new reagents/analytic tools; M.R.K.A., Y.W., Y.T., T.H., and M.A.E.-S. analyzed data; and M.R.K.A., Y.W., N.F., R.W., and M.A.E.-S. wrote the paper.

Reviewers: B.M.R., Boston University; and W.T., University of Florida.

The authors declare no conflict of interest.

[1]M.R.K.A. and Y.W. contributed equally to this work.

[2]To whom correspondence may be addressed. Email: melsayed@gatech.edu, nfang@gsu.edu, or ronghu.wu@chemistry.gatech.edu.

This article contains supporting information online at www.pnas.org/lookup/suppl/doi:10.1073/pnas.1703151114/-/DCSupplemental.

cancer cell migration. Therefore, a complete scope of the mechanism of nanoparticles' effect on the cytoskeletal proteins needs to be explored by systematic biological strategy.

In general, it has been reported that heat stress affects the cytoskeleton and induces its rearrangements (27–29). Thus, we hypothesized that the use of AuNRs allows us to apply near-infrared (NIR) laser to generate heat efficiently through nonradiative processes (13, 30, 31). AuNRs, due to their unique chemical, physical, and optical properties, have been used in drug delivery (32), bioimaging, and PPTT of cancer (33–36). NIR light is a low energetic (safe) light that can deeply penetrate the tissues, which could potentially enhance the AuNRs' effects on cytoskeletal proteins and inhibit migration.

Integrins are major adhesion and signaling receptor proteins that play an important role in regulating cytoskeleton (37, 38) by providing a physical linkage between the cytoskeleton and the extracellular matrix (ECM) and receiving signals from the ECM (39). They could perturb the downstream cell adhesion and migration pathways and modulate the cytoskeleton, thus regulating cell motility and migration (40, 41). Numerous studies have reported differentially expressed integrins in many cancers. Integrins $\alpha_v\beta_3$, $\alpha_5\beta_1$, and $\alpha_v\beta_6$ are found in very low abundance, even undetectable levels, in most adult epithelial cells, whereas they can be highly overexpressed in many tumors (42). Integrins are also regulators of metastasis. For instance, inducing the expression of the $\alpha_v\beta_3$ integrin subunit in cancer cell lines increases their metastatic potential (43, 44). The Arg–Gly–Asp (RGD) peptides are known for specific binding to a wide number of surface integrins, including $\alpha_v\beta_3$, $\alpha_3\beta_1$, and $\alpha_5\beta_1$ integrins (45–47). The good selectivity of RGD to cancer cells has been reported by numerous studies for delivering nanoparticles to cancer cells or tumors (48).

To overcome the drawbacks of using nanoparticles, four aspects of the nanoparticle design have been considered to achieve more effective inhibition of cancer cell migration: (*i*) lowering the concentration of nanoparticles to nM dosage, as a means for lowering toxicity; (*ii*) enhancing the selectivity to the cancerous cells; (*iii*) applying NIR light to enhance the AuNRs' effects on cytoskeletal proteins to inhibit migration; and (*iv*) most importantly, enhancing the migration inhibition effect by targeting AuNRs to integrin proteins to remodel the cytoskeleton with systematic understanding of the mechanism behind. In our work, RGD peptides were conjugated on the surface of AuNRs to achieve the selective targeting of integrin. NIR light was applied to the AuNRs to generate mild heat. The concentration of the AuNRs and heat were kept well below the threshold to avoid negative effects on cell viability or proliferation. We compared both nontargeted and integrin-targeted AuNRs (AuNRs@RGD). Results indicated that although both types of AuNRs decreased the cell migration speed, the targeted ones did so with a greater effect. After applying NIR light, cell motility was further decreased. We have performed a proteomics study to understand the molecular mechanism, explaining how and why AuNRs have a wide range of effects in perturbing cytoskeletal proteins and cell migration pathways. Compared with the drugs composed of small molecules that target only a single protein, AuNRs exhibit great promise as an antimetastasis strategy for clinical use.

Results

AuNR Fabrication, Characterization, Cell Uptake, and Cytotoxicity Study. AuNRs with a size of 25 (±3) × 6 (±1) nm (length × width) and aspect ratio of 4.2 were synthesized according the seedless method (49), as shown in the transmission electron microscope (TEM) in Fig. 1*A*. This size of AuNRs has shown better efficacy in heat generation in PPTT by our previous study (50). The as-synthesized AuNRs were washed twice with water to remove cetyltrimethylammonium bromide (CTAB) to decrease the cytotoxicity and for the next step of surface modification. The AuNPs were functionalized with polyethylene glycol thiol (PEG) and RGD peptides to increase the biocompatibility (51) and achieve integrin targeting (45), respectively. Surface modification causes a red shift of the longitudinal surface plasmon resonance (SPR) band of AuNRs due to the change in the dielectric constant of the surrounding environment of AuNRs (as shown in the UV-Vis spectra in Fig. 1*B*). After PEGylation, the SPR band red-shifts to 785 nm for AuNRs@PEG (initially 771 nm). Further red-shift to 796 nm for AuNRs@RGD was observed, indicating the surface binding of RGD. In addition, the zeta potentials of the AuNRs at different stages were measured to confirm the surface modifications. As shown in Fig. 1*C*, the as-synthesized CTAB-coated AuNRs had a positive surface charge of 22.9 ± 15.1 mV, as the CTAB is a highly cationic surfactant. After PEG modification, the AuNRs became negatively charged (–10.2 ± 6.73 mV) and then became positive again after further modification of the RGD peptides. The characterization results are consistent with previous reports (52, 53), which indicates the successful conjugation of the RGD peptides to the surface of AuNRs.

Successful internalization of AuNRs within the cells was observed as monitored under a dark-field (DF) microscope (Fig. 1 *D–F* and Fig. S1), where the brightness of the scattering light from AuNRs indicates the internalized AuNR amount. The human oral squamous cell carcinoma (HSC-3) cells were incubated with 2.5 nM of AuNRs for 24 h. For AuNRs@RGD, clear scattering light of AuNRs was observed, whereas AuNRs@PEG did not show high uptake compared with the AuNRs@RGD. The difference in uptake of these two types of AuNRs is due to the binding of RGD to the surface integrin that enhances the endocytosis of AuNRs (54). For further confirmation, the internalization of AuNRs was also measured by UV-Vis spectra (Fig. S2*A*) and the differential interference contrast (DIC) microscopy (Fig. S2 *B–D*). In addition, the retention of the Gaussian-shape peaks in the UV-Vis spectra of AuNRs after incubation with cells indicates the colloidal stability. Flow cytometry was used to measure the cell viability and apoptosis status, and the results indicated 2.5 nM AuNRs@PEG and AuNRs@RGD did not affect the cell viability or cause apoptosis (Fig. 1*G* and Fig. S3). This result confirms that the functionalization of AuNRs has been well performed by ligand–ligand exchange to replace the CTAB with PEG and RGD. A 808-nm CW NIR laser was applied for 1 min to raise the temperature of the culture media to about 42 ± 1 °C. As the temperature increased, there was no obvious change in the cell viability and no sign of apoptosis/necrosis (Fig. 1 *G–K* and Fig. S3). In addition, no cell apoptosis occurred after AuNR incubation and slight NIR exposure, as confirmed by our Western-blot results (Fig. 1*L*). BAX, an important protein that participates in the initiation of apoptotic signaling (55), did not increase.

AuNRs Inhibit Cancer Cell Migration and Invasion Ability. To evaluate the AuNRs' effect on cancer cell migration, we conducted a scratch assay (56) on the monolayers of cells that were incubated with or without AuNRs for 24 h. After introducing a "scratch" or "wound" into a cell culture, images were captured immediately and 12 h after the scratch. Fig. 2*A* and Fig. S4*A* indicate that cells in the control group had the wound completely healed, whereas cells treated with AuNRs were not completely healed. The integrin-targeting AuNRs (AuNRs@RGD) have a greater inhibition effect than the nontargeted AuNRs (AuNRs@PEG). In addition, NIR light exposure demonstrated an enhanced inhibition effect on cancer cell migration.

As mentioned above, the cell motility decreased upon the AuNR treatment. It is well known that changes in cell morphology are closely related to cell motility, which is initiated through two types of membrane protrusions: flat, sheet-like lamellipodia and needle-like, actin-based filopodia (Fig. 2*B*). Both structures contain a large density of integrins (57) and play major roles in leading cancer cell migration and invasion (58, 59). To study the cell morphological changes (lamellipodia and filopodia), a DIC microscope was used. The control sample exhibited a normal and extended lamellipodia

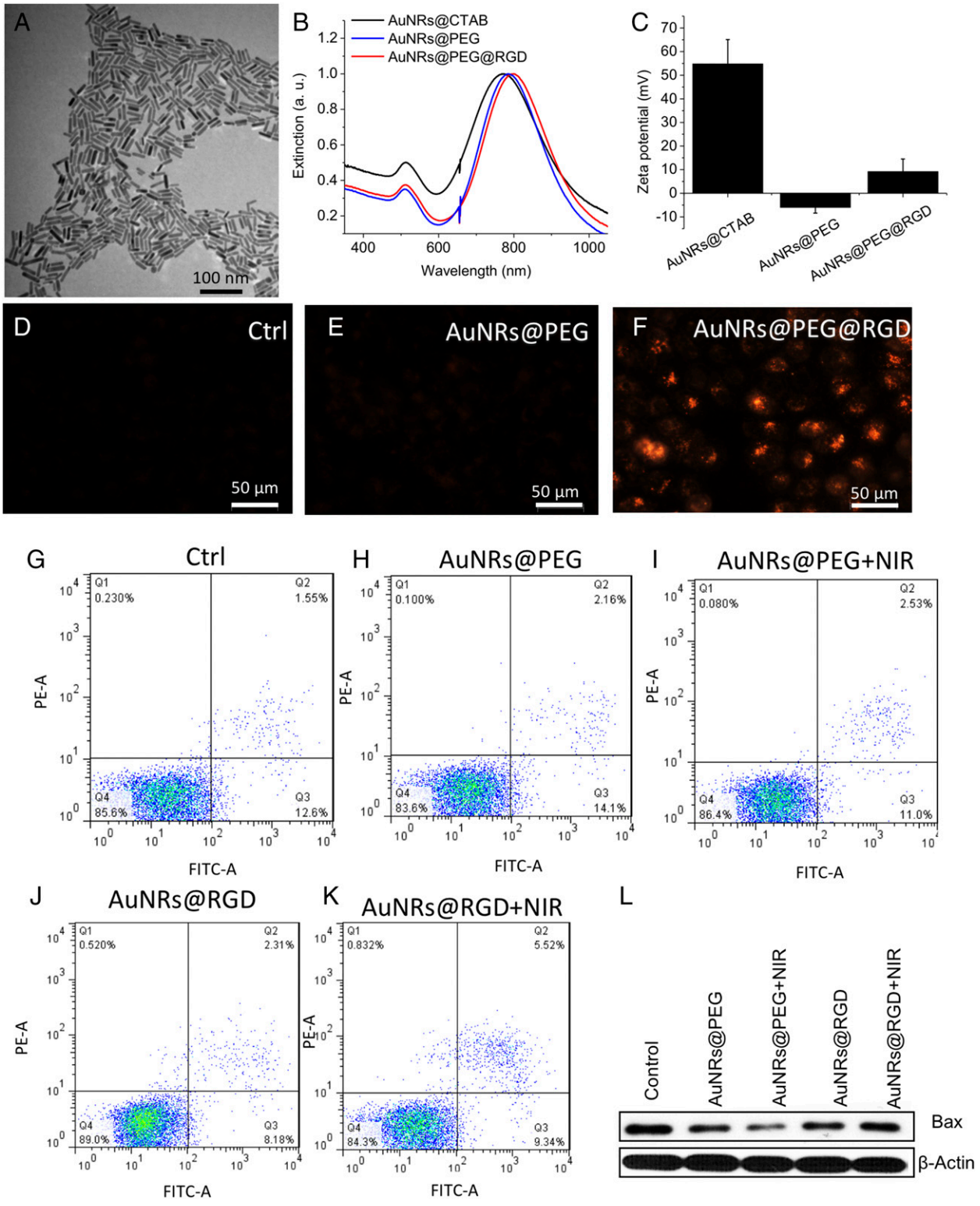

Fig. 1. AuNR synthesis, characterization, HSC-3 cellular uptake, and cytotoxicity study. (*A*) TEM image of AuNRs. (*B*) UV-Vis spectrum of AuNRs with different surface ligands. Black, the as-synthesized AuNRs with CTAB on the surface; blue, PEGylated AuNRs; red, AuNRs conjugated with PEG and RGD. (*C*) Zeta potential shows the surface charge before/after conjugations. (*D–F*) DF image of cells without AuNRs, incubated with AuNRs@PEG or AuNRs@RGD, respectively (representative of replicated experiments, another two sets of results in Fig. S1). (*G–K*) Cell viability/apoptosis/necrosis assay of cells under different treatments, using flow cytometry. Q1, necrotic cells; Q2, late apoptotic cells; Q3, early apoptotic cells; Q4, viable cells (representative of replicated experiments, statistical results in Fig. S3). (*L*) Western blotting for the BAX protein after four groups of treatments.

and filopodia. After treating with AuNRs@RGD alone, the cells tended to have a round shape with fewer lamellipodia and filopodia compared with the control. When we applied AuNRs@RGD and NIR light together, the area of lamellipodia was further decreased,

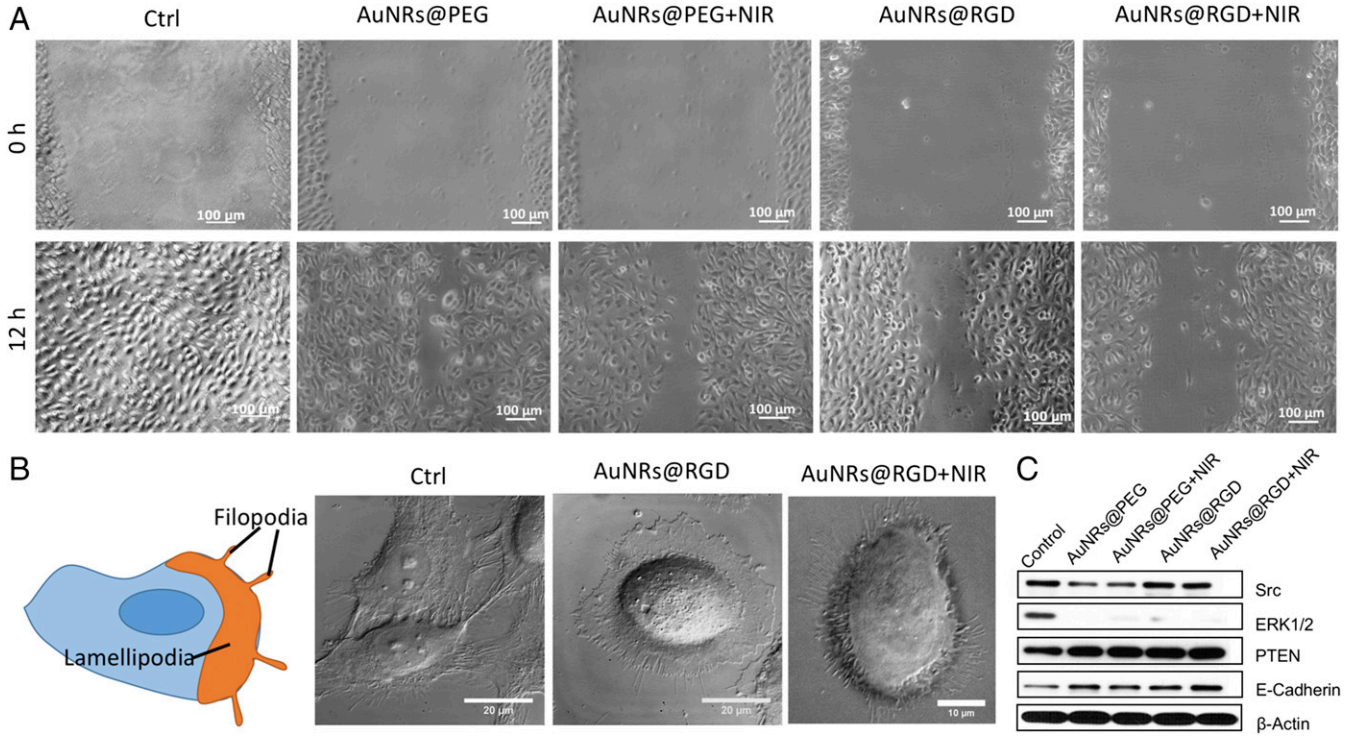

Fig. 2. Changes of cell migration rate and shapes upon AuNRs treatments. (*A*) Images of HSC cell movement using scratch assay (representative of replicated experiments, another set of results in Fig. S4*A*). (*B*) Changes in the cell shape using DIC images before and after AuNR or NIR treatments (representative of replicated experiments, another set of results in Fig. S4*B*). (*C*) Western-blot analysis of integrin- and migration-related proteins in AuNRs@PEG and AuNRs@RGD (with or without NIR light).

and many needle-like filopodia appear outside the cell (more information is available in Fig. S4*B* and Movie S1). The morphological changes of integrin-rich lamellipodia and filopodia indicate that the integrin-targeted AuNRs with or without NIR light are effective in changing the cytoskeleton structures, a probable cause for the decrease in cell motility.

To study the molecular mechanism, we checked the expression levels of several proteins that are closely associated with integrin and cell migration. Two important downstream regulators of integrin, Src and ERK1/2, were found to be down-regulated with the AuNR treatment compared with the control (Fig. 2*C*). Src is a critical protein that bridges between integrin and Rho (a main regulator of cytoskeleton) signaling (60), and ERK1/2 is a mitogen-activated protein kinase (61, 62). The decrease of Src and ERK1/2 indicates that targeting the surface integrin using AuNRs@RGD might block the downstream regulators of integrin signaling (63), which contributes to the inhibition of cell migration by AuNRs. Moreover, in a further investigation of integrin-related proteins, Fig. 2*C* showed that epithelial cadherin (E-cadherin) and phosphatase and tensin homolog (PTEN) were up-regulated upon AuNR treatments. Recent discoveries have shown that E-cadherin has cross-talks with integrin signaling (64) that alter cytoskeletal organization (65). Loss of E-cadherin is often associated with tumor invasive progressing (66). In addition, the tumor suppressor protein PTEN has been reported to inhibit integrin-mediated cell migration, spreading, and adhesion and affect mitogen-activated protein kinase (67–69). Our results indicated that the up-regulation of E-cadherins and PTEN contributes to the inhibition of cancer migrations.

Proteomics Analysis Reveals the Inhibition of Migration Pathways. To gain a global view of proteome change, label-free quantitative proteomics was conducted to identify and quantify protein expression changes in HSC-3 cells after incubation with AuNRs. Proteomics results indicated a wide range of perturbations of proteins in migration-related pathways after AuNR treatment. In this experiment, cells were lysed and proteins were then extracted and digested. The purified peptides were analyzed by an online liquid chromatography–mass spectrometry (LC-MS) system. Two biological replications and three technical replications for each condition were conducted. In total, over 4,000 proteins were identified, and about 1,800 common proteins were quantified in four treatment groups (AuNRs@PEG, AuNRs@PEG+NIR, AuNRs@RGD, and AuNRs@RGD+NIR) (Fig. 3*A*). The clustering analysis (Fig. S5 *A* and *B*) shows that the control group and experimental groups were separately clustered, also indicating a good reproducibility of the proteomics experiments. Differential analysis identified proteins with significant changes in AuNR-treated groups compared with the control group (Fig. S5 *C*–*F*). The numbers of up- and down-regulated proteins in each group are shown in Fig. S5*G*. Comparison of differentially expressed proteins identified in the four treatments is shown in the Venn diagram (Fig. S5*H*). Expression levels of key proteins in migration-related pathways are shown in the heatmap (Fig. 3*B*), where a wide range of cytoskeletal proteins were observed to be affected in the four AuNR-treated groups. Pathway analysis using MetaCore (Thomson Reuters) reveals the perturbation of signaling pathways related to cell migration in all groups (Fig. 3*C*), including the cytoskeleton remodeling, Rho GTPase signaling, integrin-mediated cell migration and invasion, etc. Maps of these pathways are shown in Fig. S6. Per the pathway analysis results, AuNRs@RGD+NIR caused the greatest changes to the migration-related pathway and was considered the most effective for inhibiting cancer cell migration, followed by AuNRs@RGD and then AuNRs@PEG.

A scheme (Fig. 4) was concluded from the pathway maps (Fig. S6) to illustrate the changes of the key protein players in the migration-related pathways. AuNRs regulate the cell migration by affecting the cytoskeleton in four main ways: (*i*) Rho GTPases, (*ii*) actin, (*iii*) microtubule, and (*iv*) kinase-related signaling pathways.

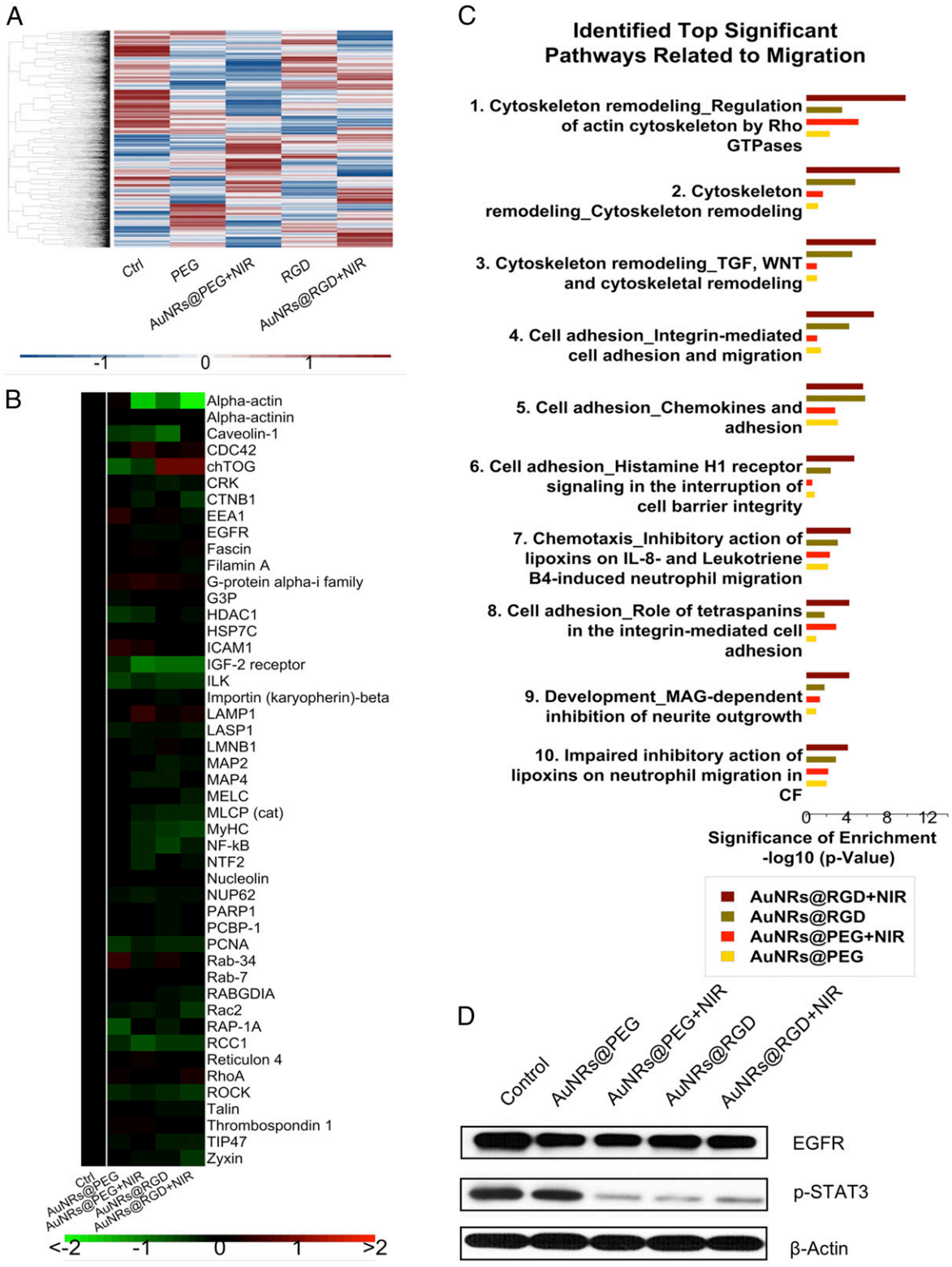

Fig. 3. Experimental results of proteomics in the four treatment groups (AuNRs@PEG, AuNRs@PEG+NIR, AuNRs@RGD, and AuNRs@RGD+NIR). (*A*) Heatmap showing the expression levels of all of the quantified proteins. (*B*) Heatmap showing identified proteins contributing to migration inhibition. (*C*) Bar graph showing identified significant pathways related to migration. (*D*) Western-blot analysis of some integrin- and migration-related proteins.

i) Rho GTPases regulate the actin cytoskeleton (70–72), which plays an important role in cellular contractility (actomyosin contraction) by directly controlling the balance between myosin II and actin and initiates the force needed for cell migration (73–75). Many key proteins in Rho GTPase signaling pathways were perturbed, including serine/threonine kinase ROCK, myosin heavy chain (MyHC), myosin essential light chain (MELC), myosin light-chain phosphorylation

(MLCP), RhoA, α-actinin, talin, etc., as shown in Figs. 3*B* and 4. All four treatments exhibit the regulation of Rho GTPase signaling to different extents. The AuNRs@RGD+NIR group has the highest statistical significance with the lowest *P* value (1.5×10^{-10}), reflecting this group's highest efficacy in inhibiting the cancer cell migration-related pathways. Our results indicate the disruption of actomyosin contraction, which might prevent the generation of traction force during the migration process.

ii) In addition to disrupting actomyosin contraction, the effect of AuNRs on focal adhesions (or cell-matrix adhesion) was also observed. Focal adhesions are related to integrins and other associated proteins, which form links between intracellular actin cytoskeleton and ECM (76). The activated integrins couple to the actin cytoskeleton by recruiting actin-binding proteins (77). Our results show that actin-binding proteins, including alpha-actinin, talin, and vinculin, were down-regulated after AuNRs incubation (Figs. 3*B* and 4), suggesting the connectivity between integrin and actin cytoskeleton was likely weakened due to the blocking effect of AuNRs on the migration pathways.

iii) Although the actin cytoskeleton provides contractile forces, microtubules form a polarized network throughout the cell. The microtubule-associated proteins (MAPs) were significantly down-regulated (MAP2 and MAP4), indicating the rearrangement of microtubules. MAPs bind directly to the tubulin dimers of microtubules, which often leads to the stabilization and polymerization of microtubules (78). The disruption of the intracellular microtubule assembly could also limit the cell motility (79).

iv) Furthermore, our results show several kinases related to the integrin signaling pathways were perturbed, including integrin-linked kinase (ILK), nuclear factor-κB (NF-κB), the epidermal growth factor receptor (EGFR), caveolin, etc. These proteins are closely associated with integrin regulation and cell migration (80). It has been reported that the overexpression of ILK could promote the migration and invasion of colorectal cancer cells via NF-κB signaling (81). In the current results, the down-regulation of ILK and NF-κB is associated with reduced cancer cell migration ability. In addition, the expression level of EGFR, a surface receptor for epidermal growth factor, decreased. The down-regulation of EGFR was also confirmed in the Western-blot results. EGFR is regarded as an important target for anticancer therapeutics (82). Furthermore, STAT3, which is normally activated by tyrosine phosphorylation in response to the addition of EGFR (83) and can promote cell migration, was also down-regulated in all of the AuNR-treated samples (Fig. 3*D*).

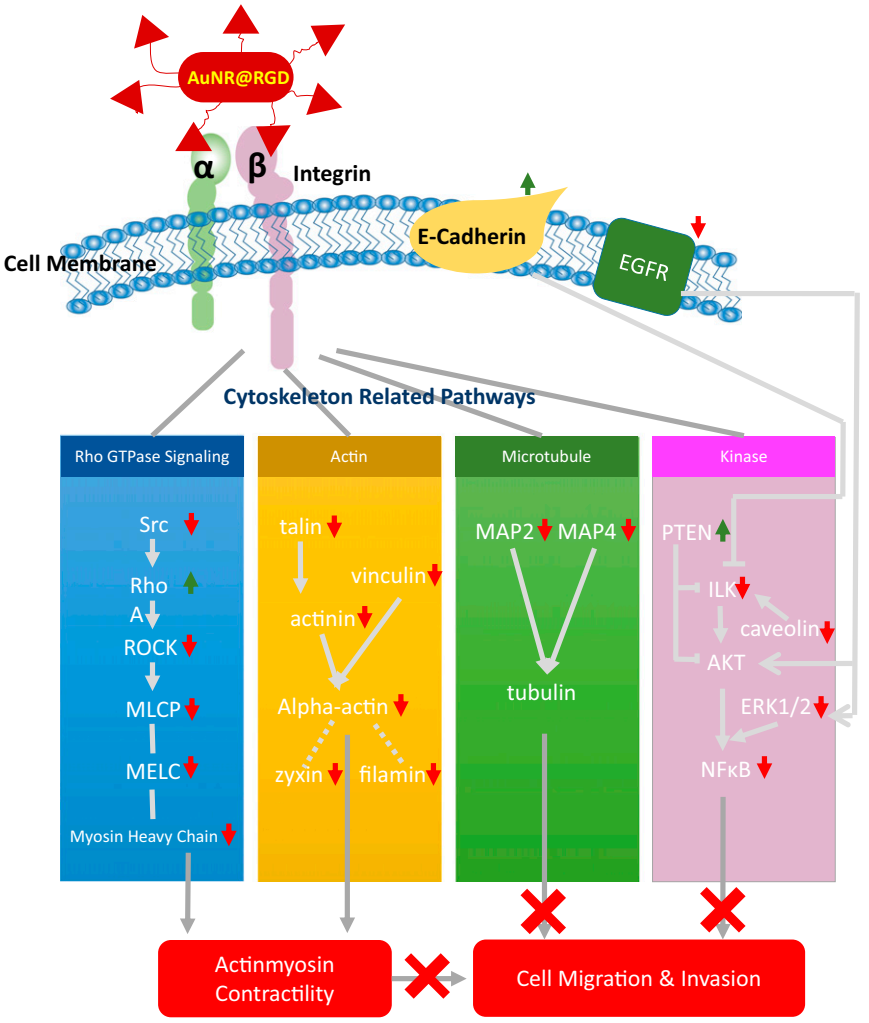

Fig. 4. Scheme representing the mechanisms involved in inhibiting cell migration upon AuNR treatments. When the AuNRs@RGD (in red) target the alpha/beta integrins, four different cytoskeletal proteins pathways are regulated, Rho (blue), Actin (yellow), Microtubule (green), and Kinase (pink), all of which affect the cell contractility and thus inhibit cell migration (shown in red at the bottom of the figure).

Discussion

Current advances of nanoscience and nanomedicine enable us to fabricate "intelligent" nanomaterials that can specifically target cellular and subcellular locations in living animals for treating diseases (84, 85). Although larger nanoparticles (>18 nm in diameter) can accumulate in organs such as the liver and spleen and be eliminated slowly (86), the long-term effect of AuNRs in mice shows no toxic effect after 15 mo (87). The biocompatibility and special physicochemical properties of AuNRs provide us an effective and safe potential treatment of cancer.

Our previous study has shown success in treating xenograft mice and natural mammary gland tumors in dogs and cats using AuNR-assisted PPTT, where no cancer relapse or metastasis occurred in any of the test subjects (87, 88), implying the potential effect of AuNRs in inhibiting cancer metastasis. We also designed nuclear membrane-targeted AuNPs for inhibiting cancer cell migration and invasion, by mechanically increasing their nuclear stiffness, with greatly reduced AuNP dosage (26). Herein, we reported that targeting AuNRs to cancer cell surface integrins could greatly rearrange the cytoskeleton proteins, thus enhancing the inhibition effect on cancer cell migration. Compared with nontargeted AuNRs, the integrin-targeted AuNRs are more effective on cell migration inhibition with a nanoparticle concentration at the nM scale (1,000× lower than the literature values) (18, 19, 22), which could be safer for future clinical use.

Our result shows that cancer cells incubated with integrin-targeted AuNRs (with or without NIR light exposure) exhibited impaired migration abilities. Morphological changes were observed in cytoskeleton protrusions by targeting surface integrins using AuNRs, namely lamellipodia and filopodia, that form the leading edge for cell movement. These cytoskeleton protrusions were reduced after treating the cells with AuNRs@RGD. Furthermore, greater morphological changes were observed after applying NIR light. Integrins are often found in the tips or alone in the shaft of filopodia and lamellipodia, which creates the "sticky fingers" and facilitates the migration and invasion (89, 90). The reason for this morphological change has been explored in our Western blot and proteomics analysis, which indicated that the integrin-related proteins were obviously affected.

In addition to the morphological change through lamellipodia and filopodia, systematic molecular mechanisms have been studied, and many protein pathways exhibit changes after exposure to integrin-targeted AuNRs. This broad change of cytoskeletal proteins is possibly due to the ability of integrin in controlling cytoskeleton through many different ways as an up-stream surface receptor. Results show that by targeting surface integrins, the focal adhesion connecting the cytoskeleton to the ECM through integrin might be weakened. Moreover, the actomyosin contraction, which creates intracellular tension for migration, has been modulated through the Rho GTPase signaling. Although targeting integrins, both the changes of actin and microtubule were observed, as well as several protein kinases that related to cytoskeleton and cancer progression and metastasis. All of the above aspects could finally result in the inhibition of cancer cell migration.

In summary, the ability of targeting AuNRs to cancer cell surface integrins and the introduction of PPTT caused wide-range regulation on cytoskeletal proteins, observed as lamellipodia/filopodia morphological changes and four major groups of migration-related protein changes. Applying NIR light to generate mild heat further enhanced this effect. This strategy provides a potential application for controlling cancer metastasis. Future work will be focused on testing the effect of AuNPs on preventing and treating cancer metastasis in animals. The injection method (either active or passive tumor targeting) should be decided, and more investigation will be conducted.

Methods

Materials. Tetrachloroauric acid trihydrate ($HAuCl_4.3H_2O$), $NaBH_4$, ascorbic acid, CTAB, $AgNO_3$, 4-(2- hydroxyethyl)-1-piperazineethanesulfonic acid (Hepes), NaCl, sodium deoxycholate, SDS, and Triton × 100 were purchased from Sigma-Aldrich. Methoxypolyethylene glycol-thiol (mPEG-SH, MW 5000) was purchased from Laysan Bio, Inc. Cell-penetrating peptide RGD (RGDRGDRGDRGDPGC) was obtained from GenScript, Inc. Dulbecco's PBS, DMEM, FBS, antibiotic solution, and 0.25% trypsin/2.2 mM EDTA solution were purchased from VWR. Mammalian cell protease inhibitors and phosphatase inhibitors were purchased from Roche Applied Sciences, and sequencing grade trypsin was purchased from Promega. Lysyl endopeptidase (Lys-C) was purchased from Wako.

Instrumentation. AuNPs were imaged using a JEOL 100CX-2 TEM, and their average size was then measured by ImageJ software. UV-vis spectra were obtained using an Ocean Optics HR4000CG UV-NIR spectrometer. An inverted Nikon Eclipse Ti-E microscope equipped with Perfect Focus System (PFS, 25 nm *z* axial resolution) was used for imaging under a Nikon DIC microscope. Proteomics analysis was performed on a hybrid dual-cell quadrupole linear ion trap–Orbitrap mass spectrometer LTQ Orbitrap Elite (Thermo Fisher) with XCalibur 3.0.63 software. Flow cytometry experiments were conducted on a BD LSR II Flow Cytometer (BD Biosciences).

Synthesis, Conjugation, and Characterization of AuNRs. AuNRs with an average size of 25 × 6 nm (length × width) were synthesized using a seedless growth method (49). We added 5 mL of 1.0 mM $HAuCl_4$ to a solution of 5 mL of 0.2 M CTAB, 250 μL of 4.0 mM $AgNO_3$, and 8 μL of 37% HCl. Then, 70 μL of 78.8 mM ascorbic acid was added, followed by immediate injection of 15 μL of 0.01 M ice-cold $NaBH_4$. The solution was left undisturbed for 12 h. The particles were centrifuged at 21,000 × *g* for 50 min and dispersed in DI water, followed by a second centrifugation at 19,000 × *g* for 40 min to remove the extra CTAB. TEM was used to measure the sizes and homogeneity of the nanoparticles.

After rinsing them with water, AuNRs were then conjugated with different surface ligands (PEG and RGD). For AuNRs@PEG, mPEG-SH (1 mM) was added to the nanoparticles overnight to achieve about 5,000 ligands on each particle. For preparing AuNRs@RGD, first, mPEG-SH (1 mM) was added to the nanoparticles overnight to achieve about 1,000 ligands on each particle. Then, the PEGylated nanoparticles (1 nM) were treated with RGD (1 mM) to achieve 10,000 molar excess. The solution was then allowed to shake overnight at room temperature. Excess of ligands was removed by centrifugation. UV-vis spectrometer and zetasizer were used to test the conjugation.

Cell Culture, AuNR Treatments, and PPTT. The human oral squamous cell carcinoma (HSC-3) cells were grown in DMEM (Mediatech) containing 10% (vol/vol) FBS (Mediatech) and 1% antimycotic solution (Mediatech) at 37 °C in a humidified incubator under 5% CO_2. Cells were cultured in 60-mm dishes for 24 h followed by incubation with AuNRs for 24 h. Then, a CW 808-nm laser (5.8 W/cm^2, spot size 5.6 mm) was applied to the cells for 1 min. To cover the entire area of the culture dish, the laser was applied spot by spot using scanning with each spot undergoing 1 min of laser exposure time. The cells were then harvested for MS analysis, with a final confluence of about 80–90%.

Sample Preparation for Proteomics Experiment. After treatment for 24 h, cells were washed twice using PBS. Cell lysates were prepared by directly adding the lysis buffer (150 mM NaCl, 50 mM Hepes, pH 7.4, 0.1% SDC, 10 units per mL benzonase, protease inhibitor mixture) to the cells followed by scraping and collecting on ice. Lysates were vortexed for 90 s (30 s × 3 times, 2 min pause), sonicated on ice, and centrifuged at 18,000 × *g* for 15 min at 4 °C. The supernatant solutions were saved, and proteins were precipitated by adding 4× excess volumes of ice-cold precipitation solvents (acetone:ethanol: acetic acid = 50:50:0.1). After centrifugation, the protein pellet was redissolved in a solution with 8 M urea and 50 mM Hepes (pH 8) (91).

Protein disulfide bonds were reduced using 1 mM DTT followed by alkylation with 5.5 mM iodoacetamide. After the lysates were diluted twice (final urea concentration of 4 M), endoproteinase Lys-C (1:100 wt/wt) was added to digest proteins for 4 h. Then, modified sequencing grade trypsin (1:100 wt/wt) was used for further digestion in a more diluted solution with the final urea concentration of 1 M overnight (92). Protein concentration was measured by Bradford assay.

RPLC–MS/MS Analysis for Label-Free Quantitative Proteomics. The proteomics analysis was conducted using the previously reported method (53). Briefly, purified and dried peptide samples from the previous step were dissolved in 10 μL solvent with 5% acetonitrile and 4% FA, and 4 μL of the resulting

solutions were loaded onto a microcapillary column packed with C18 beads (Magic C18AQ, 3 μm, 200 Å, 100 μm × 16 cm, Michrom Bioresources) by a Dionex WPS-3000TPLRS autosampler (UltiMate 3000 thermostated Rapid Separation Pulled Loop Well Plate Sampler). A reversed-phase liquid chromatography (RPLC) was used for peptide separation with a 110-min gradient of 8–38% ACN (with 0.125% FA). Peptides were detected with a data-dependent Top20 method—that is, for each cycle, one full MS scan (resolution, 60,000) in the Orbitrap was followed by up to 20 MS/MS in the ion trap for the most intense ions. The selected ions were excluded from further analysis for 90 s. Ions with singly or unassigned charge were not sequenced. Maximum ion accumulation times were 1,000 ms for each full MS scan and 50 ms for MS/MS scans. The sample at each condition was repeated 6 times (2 biological and 3 technique replicates) for label-free quantification.

Apoptosis/Necrosis Assay. After removing the cell culture media, cells were washed with PBS and collected after trypsinization followed by washing with cold PBS twice again. Then, the cells were dispersed in a mixture of 493 mL of annexin V binding buffer, 5 μL of annexin V FITC (BioLegend), and 2 μL of propidium iodide PI (BioLegend, 100 μg/mL) and incubated for 15 min at room temperature. The cells were then filtered and subjected to flow cytometry analysis using a BSR LSR II flow cytometer (BD Biosciences). A 488-nm laser was applied for excitation, and FITC was detected in FL-1 using a 525/30 BP filter, whereas PI was detected in FL-2 using a 575/30 BP filter. Standard compensation using unstained and single-stained cells was done before running actual experiments. FlowJo software (Tree Star Inc.) was used for analysis of the viable, apoptotic, and necrotic cells from at least 10,000 events.

Cell Imaging Using DIC Microscopy. The Nikon DIC mode used a pair of polarizer and analyzer, a high-resolution 100×I-R Nomarski DIC slider, a high numerical aperture (N.A., 1.40) oil immersion condenser lens, a Nikon CFI Apo TIRF 100× (N.A., 1.49) oil immersion objective, and a 12 V/100 W halogen lamp as the light source. Appropriate bandpass filters were placed in the light path. Fixed HEYA8 cells on 22 mm × 22 mm glass coverslips were rinsed with PBS at pH 7.4 and fabricated into a sandwiched chamber with two pieces of double-sided tape and a cleaned glass slide. PBS solution was then added into the chamber to fill the space, and the chamber was then sealed by clear nail polish. The so-formed sample slide was then placed under the microscope for observation. Two scientific CMOS cameras were used to capture the DIC images: a Hamamatsu C11440-22CU, ORCA-Flash 4.0 V2 with a 2048 × 2048 pixel array and a pixel size of 6.5 μm × 6.5 μm and a Tucsen Dhyana 95 with a 2048 × 2048 pixel array and a pixel size of 11 μm × 11 μm. These cameras performed similarly in our experiments.

Scratch Assay. The scratch assay has been performed according to a former report (56). Cells were cultured in a six-well plate to a confluent monolayer. A p200 pipet tip was used to scrape the cell monolayer in a straight line to create an empty gap. The debris was then removed by washing the cells once with a culture medium and then replaced with 2 mL of fresh medium. Then, the cells were imaged immediately after scratch and 12 h after scratch.

Proteomics Data Analysis. Two biological replications and three MS technical replications for each condition (control, AuNRs@PEG, AuNRs@PEG/NIR, AuNRs@RGD, AuNRs@RGD/NIR) were conducted. Raw data from proteomics was normalized using supervised normalization of the microarray (SNM) (93). In the SNM procedure, variance due to biological and technical replicates was adjusted by setting them as variables in the model. Variance explained by different experimental treatments (control, AuNRs@PEG, and AuNRs@PEG+NIR for PEG-conjugated AuNR group; control, AuNRs@RGD, and AuNRs@RGD+NIR for RGD-conjugated AuNR group) was fitted as a biological variable in the model. Hierarchical clustering was done with statistical software R. Proteomics data were log2-transformed before analysis of variance (ANOVA), which was used to detect differential expression of proteins between control and treatment groups, with treatment conditions set as fixed effects. *P* value threshold at 0.1 was set to select differential proteins. The proteins identified as being affected were subjected to pathway analysis using the MetaCore pathway analysis software ("MetaCore from Thomson Reuters").

Western Blot Analysis. Briefly, cells were lysed in RIPA buffer (20 mM Tris, pH 7.4, 150 mM NaCl, 2 mM EDTA, 2 mM EGTA, 0.1% sodium deoxycholate, 1% Triton X-100, 0.1% SDS) containing protease inhibitors (Sigma-Aldrich). BCA assay (Pierce) was performed to measure the protein concentration, and equal amounts of protein were loaded on a SDS/PAGE gel. After the protein separation, the resulting gels were transferred to PVDF membranes (Millipore) overnight. Afterward, the gel was blocked with 5% milk in TBS (20 mM Tris, 150 mM NaCl). The primary antibodies (Bethyl Laboratories, Inc.) were incubated with the membrane overnight in 4 °C with shaking, followed by adding the secondary antibodies (Jackson Immuno Research Laboratories). Blots were washed three times for 20 m in TBS after primary and secondary antibodies.

ACKNOWLEDGMENTS. We thank the El-Sayed Undergraduate Research group, including Sarah Ghalayini, Arusha Siddiqa, and Arya Moradinia, for critical proofreading of the manuscript. M.A.E. acknowledges National Science Foundation Division of Chemistry (CHE) Grant 1608801 for its support of this work; R.W. acknowledges support from National Science Foundation CAREER Award CHE-1454501; and K.C. and N.F. acknowledge funding support from NIH Grant 1R01GM115763.

1. Talmadge JE, Fidler IJ (2010) AACR centennial series: The biology of cancer metastasis: Historical perspective. *Cancer Res* 70:5649–5669.
2. Fidler IJ (2003) The pathogenesis of cancer metastasis: The 'seed and soil' hypothesis revisited. *Nat Rev Cancer* 3:453–458.
3. Chaffer CL, Weinberg RA (2011) A perspective on cancer cell metastasis. *Science* 331: 1559–1564.
4. Fife CM, McCarroll JA, Kavallaris M (2014) Movers and shakers: Cell cytoskeleton in cancer metastasis. *Br J Pharmacol* 171:5507–5523.
5. Hanahan D, Weinberg RA (2011) Hallmarks of cancer: The next generation. *Cell* 144: 646–674.
6. Dumontet C, Jordan MA (2010) Microtubule-binding agents: A dynamic field of cancer therapeutics. *Nat Rev Drug Discov* 9:790–803.
7. Stehn JR, et al. (2013) A novel class of anticancer compounds targets the actin cytoskeleton in tumor cells. *Cancer Res* 73:5169–5182.
8. Patel RA, Liu Y, Wang B, Li R, Sebti SM (2014) Identification of novel ROCK inhibitors with anti-migratory and anti-invasive activities. *Oncogene* 33:550–555.
9. Prudent R, et al. (2012) Pharmacological inhibition of LIM kinase stabilizes microtubules and inhibits neoplastic growth. *Cancer Res* 72:4429–4439.
10. Banerjee S, Hwang DJ, Li W, Miller DD (2016) Current advances of tubulin inhibitors in nanoparticle drug delivery and vascular disruption/angiogenesis. *Molecules* 21:E1468.
11. Morgillo F, Lee HY (2005) Resistance to epidermal growth factor receptor-targeted therapy. *Drug Resist Updat* 8:298–310.
12. Holohan C, Van Schaeybroeck S, Longley DB, Johnston PG (2013) Cancer drug resistance: An evolving paradigm. *Nat Rev Cancer* 13:714–726.
13. Murphy CJ, et al. (2008) Gold nanoparticles in biology: Beyond toxicity to cellular imaging. *Acc Chem Res* 41:1721–1730.
14. Moghimi SM, Hunter AC, Murray JC (2005) Nanomedicine: Current status and future prospects. *FASEB J* 19:311–330.
15. Petros RA, DeSimone JM (2010) Strategies in the design of nanoparticles for therapeutic applications. *Nat Rev Drug Discov* 9:615–627.
16. Hirsch LR, et al. (2003) Nanoshell-mediated near-infrared thermal therapy of tumors under magnetic resonance guidance. *Proc Natl Acad Sci USA* 100:13549–13554.
17. Peer D, et al. (2007) Nanocarriers as an emerging platform for cancer therapy. *Nat Nanotechnol* 2:751–760.
18. Tay CY, et al. (2014) Nanoparticles strengthen intracellular tension and retard cellular migration. *Nano Lett* 14:83–88.
19. Soenen SJH, Nuytten N, De Meyer SF, De Smedt SC, De Cuyper M (2010) High intracellular iron oxide nanoparticle concentrations affect cellular cytoskeleton and focal adhesion kinase-mediated signaling. *Small* 6:832–842.
20. Arvizo RR, et al. (2013) Inhibition of tumor growth and metastasis by a self-therapeutic nanoparticle. *Proc Natl Acad Sci USA* 110:6700–6705.
21. Yang JA, Phan HT, Vaidya S, Murphy CJ (2013) Nanovacuums: Nanoparticle uptake and differential cellular migration on a carpet of nanoparticles. *Nano Lett* 13: 2295–2302.
22. Zhou T, et al. (2014) Inhibition of cancer cell migration by gold nanorods: Molecular mechanisms and implications for cancer therapy. *Adv Funct Mater* 24:6922–6932.
23. Yildirimer L, Thanh NTK, Loizidou M, Seifalian AM (2011) Toxicology and clinical potential of nanoparticles. *Nano Today* 6:585–607.
24. Lin W, Huang YW, Zhou XD, Ma Y (2006) In vitro toxicity of silica nanoparticles in human lung cancer cells. *Toxicol Appl Pharmacol* 217:252–259.
25. Pan Z, et al. (2009) Adverse effects of titanium dioxide nanoparticles on human dermal fibroblasts and how to protect cells. *Small* 5:511–520.
26. Ali MRK, et al. (2017) Nuclear membrane-targeted gold nanoparticles inhibit cancer cell migration and invasion. *ACS Nano* 11:3716–3726.
27. Parrotta L, Faleri C, Cresti M, Cai G (2016) Heat stress affects the cytoskeleton and the delivery of sucrose synthase in tobacco pollen tubes. *Planta* 243:43–63.
28. Coakley WT (1987) Hyperthermia effects on the cytoskeleton and on cell morphology. *Symp Soc Exp Biol* 41:187–211.
29. Gavrilova LP, Korpacheva II, Semushina SG, Yashin VA (2013) Heat shock induces simultaneous rearrangements of all known cytoskeletal filaments in normal interphase fibroblasts. *Cell Tissue Biol* 7:54–63.
30. Dickerson EB, et al. (2008) Gold nanorod assisted near-infrared plasmonic photothermal therapy (PPTT) of squamous cell carcinoma in mice. *Cancer Lett* 269:57–66.
31. Huang X, El-Sayed IH, Qian W, El-Sayed MA (2006) Cancer cell imaging and photothermal therapy in the near-infrared region by using gold nanorods. *J Am Chem Soc* 128:2115–2120.
32. Ali HR, et al. (2016) Gold nanorods as drug delivery vehicles for rifampicin greatly improve the efficacy of combating Mycobacterium tuberculosis with good biocompatibility with the host cells. *Bioconjug Chem* 27:2486–2492.

33. Wang J, et al. (2012) Assembly of aptamer switch probes and photosensitizer on gold nanorods for targeted photothermal and photodynamic cancer therapy. *ACS Nano* 6: 5070–5077.
34. Ali MR, Ali HR, Rankin CR, El-Sayed MA (2016) Targeting heat shock protein 70 using gold nanorods enhances cancer cell apoptosis in low dose plasmonic photothermal therapy. *Biomaterials* 102:1–8.
35. Sugimoto H, et al. (2015) Plasmon-enhanced emission rate of silicon nanocrystals in gold nanorod composites. *ACS Photonics* 2:1298–1305.
36. Nikoobakht B, El-Sayed MA (2003) Preparation and growth mechanism of gold nanorods (NRs) using seed-mediated growth method. *Chem Mater* 15:1957–1962.
37. DeMali KA, Wennerberg K, Burridge K (2003) Integrin signaling to the actin cytoskeleton. *Curr Opin Cell Biol* 15:572–582.
38. Ridley AJ, et al. (2003) Cell migration: Integrating signals from front to back. *Science* 302:1704–1709.
39. Howe A, Aplin AE, Alahari SK, Juliano RL (1998) Integrin signaling and cell growth control. *Curr Opin Cell Biol* 10:220–231.
40. Chattopadhyay N, Wang Z, Ashman LK, Brady-Kalnay SM, Kreidberg JA (2003) α3β1 integrin-CD151, a component of the cadherin-catenin complex, regulates PTPmu expression and cell-cell adhesion. *J Cell Biol* 163:1351–1362.
41. Zhang F, et al. (2003) Distinct ligand binding sites in integrin alpha3beta1 regulate matrix adhesion and cell-cell contact. *J Cell Biol* 163:177–188.
42. Kren A, et al. (2007) Increased tumor cell dissemination and cellular senescence in the absence of beta1-integrin function. *EMBO J* 26:2832–2842.
43. Felding-Habermann B, Mueller BM, Romerdahl CA, Cheresh DA (1992) Involvement of integrin alpha V gene expression in human melanoma tumorigenicity. *J Clin Invest* 89: 2018–2022.
44. Filardo EJ, Brooks PC, Deming SL, Damsky C, Cheresh DA (1995) Requirement of the NPXY motif in the integrin beta 3 subunit cytoplasmic tail for melanoma cell migration in vitro and in vivo. *J Cell Biol* 130:441–450.
45. Ruoslahti E, Pierschbacher MD (1986) Arg-Gly-Asp: A versatile cell recognition signal. *Cell* 44:517–518.
46. Ruoslahti E (1996) RGD and other recognition sequences for integrins. *Annu Rev Cell Dev Biol* 12:697–715.
47. Humphries JD, Byron A, Humphries MJ (2006) Integrin ligands at a glance. *J Cell Sci* 119:3901–3903.
48. Han HD, et al. (2010) Targeted gene silencing using RGD-labeled chitosan nanoparticles. *Clin Cancer Res* 16:3910–3922.
49. Ali MRK, Snyder B, El-Sayed MA (2012) Synthesis and optical properties of small Au nanorods using a seedless growth technique. *Langmuir* 28:9807–9815.
50. Mackey MA, Ali MR, Austin LA, Near RD, El-Sayed MA (2014) The most effective gold nanorod size for plasmonic photothermal therapy: Theory and in vitro experiments. *J Phys Chem B* 118:1319–1326.
51. Prencipe G, et al. (2009) PEG branched polymer for functionalization of nanomaterials with ultralong blood circulation. *J Am Chem Soc* 131:4783–4787.
52. Kang B, Austin LA, El-Sayed MA (2014) Observing real-time molecular event dynamics of apoptosis in living cancer cells using nuclear-targeted plasmonically enhanced Raman nanoprobes. *ACS Nano* 8:4883–4892.
53. Ali MRK, et al. (2016) Simultaneous time-dependent surface-enhanced Raman spectroscopy, metabolomics, and proteomics reveal cancer cell death mechanisms associated with gold nanorod photothermal therapy. *J Am Chem Soc* 138:15434–15442.
54. Kim Y-H, et al. (2011) Tumor targeting and imaging using cyclic RGD-PEGylated gold nanoparticle probes with directly conjugated iodine-125. *Small* 7:2052–2060.
55. Elmore S (2007) Apoptosis: A review of programmed cell death. *Toxicol Pathol* 35: 495–516.
56. Liang CC, Park AY, Guan JL (2007) In vitro scratch assay: A convenient and inexpensive method for analysis of cell migration in vitro. *Nat Protoc* 2:329–333.
57. Guillou H, et al. (2008) Lamellipodia nucleation by filopodia depends on integrin occupancy and downstream Rac1 signaling. *Exp Cell Res* 314:478–488.
58. Lauffenburger DA, Horwitz AF (1996) Cell migration: A physically integrated molecular process. *Cell* 84:359–369.
59. Yamaguchi H, Condeelis J (2007) Regulation of the actin cytoskeleton in cancer cell migration and invasion. *Biochim Biophys Acta* 1773:642–652.
60. Arthur WT, Petch LA, Burridge K (2000) Integrin engagement suppresses RhoA activity via a c-Src-dependent mechanism. *Curr Biol* 10:719–722.
61. Hood JD, Cheresh DA (2002) Role of integrins in cell invasion and migration. *Nat Rev Cancer* 2:91–100.
62. Huang C, Jacobson K, Schaller MD (2004) MAP kinases and cell migration. *J Cell Sci* 117:4619–4628.
63. Chen PS, et al. (2007) CTGF enhances the motility of breast cancer cells via an integrin-alphavbeta3-ERK1/2-dependent S100A4-upregulated pathway. *J Cell Sci* 120:2053–2065.
64. Canel M, Serrels A, Frame MC, Brunton VG (2013) E-cadherin-integrin crosstalk in cancer invasion and metastasis. *J Cell Sci* 126:393–401.
65. Chen A, et al. (2014) E-cadherin loss alters cytoskeletal organization and adhesion in non-malignant breast cells but is insufficient to induce an epithelial-mesenchymal transition. *BMC Cancer* 14:552.
66. Onder TT, et al. (2008) Loss of E-cadherin promotes metastasis via multiple downstream transcriptional pathways. *Cancer Res* 68:3645–3654.
67. Tamura M, et al. (1998) Inhibition of cell migration, spreading, and focal adhesions by tumor suppressor PTEN. *Science* 280:1614–1617.
68. Gu J, et al. (1999) Shc and FAK differentially regulate cell motility and directionality modulated by PTEN. *J Cell Biol* 146:389–403.
69. Gu J, Tamura M, Yamada KM (1998) Tumor suppressor PTEN inhibits integrin- and growth factor-mediated mitogen-activated protein (MAP) kinase signaling pathways. *J Cell Biol* 143:1375–1383.
70. Etienne-Manneville S, Hall A (2002) Rho GTPases in cell biology. *Nature* 420:629–635.
71. Ridley AJ, Hall A (1992) The small GTP-binding protein rho regulates the assembly of focal adhesions and actin stress fibers in response to growth factors. *Cell* 70:389–399.
72. Nobes CD, Hall A (1995) Rho, rac, and cdc42 GTPases regulate the assembly of multimolecular focal complexes associated with actin stress fibers, lamellipodia, and filopodia. *Cell* 81:53–62.
73. Friedl P, Wolf K (2003) Tumour-cell invasion and migration: Diversity and escape mechanisms. *Nat Rev Cancer* 3:362–374.
74. Parsons JT, Horwitz AR, Schwartz MA (2010) Cell adhesion: Integrating cytoskeletal dynamics and cellular tension. *Nat Rev Mol Cell Biol* 11:633–643.
75. Heasman SJ, Ridley AJ (2008) Mammalian Rho GTPases: New insights into their functions from in vivo studies. *Nat Rev Mol Cell Biol* 9:690–701.
76. Kanchanawong P, et al. (2010) Nanoscale architecture of integrin-based cell adhesions. *Nature* 468:580–584.
77. Friedl P, Gilmour D (2009) Collective cell migration in morphogenesis, regeneration and cancer. *Nat Rev Mol Cell Biol* 10:445–457.
78. Al-Bassam J, Ozer RS, Safer D, Halpain S, Milligan RA (2002) MAP2 and tau bind longitudinally along the outer ridges of microtubule protofilaments. *J Cell Biol* 157: 1187–1196.
79. Etienne-Manneville S (2004) Actin and microtubules in cell motility: Which one is in control? *Traffic* 5:470–477.
80. Bock-Marquette I, Saxena A, White MD, Dimaio JM, Srivastava D (2004) Thymosin beta4 activates integrin-linked kinase and promotes cardiac cell migration, survival and cardiac repair. *Nature* 432:466–472.
81. Yan Z, et al. (2014) Overexpression of integrin-linked kinase (ILK) promotes migration and invasion of colorectal cancer cells by inducing epithelial-mesenchymal transition via NF-κB signaling. *Acta Histochem* 116:527–533.
82. Ciardiello F, Tortora G (2003) Epidermal growth factor receptor (EGFR) as a target in cancer therapy: Understanding the role of receptor expression and other molecular determinants that could influence the response to anti-EGFR drugs. *Eur J Cancer* 39: 1348–1354.
83. Zhong Z, Wen Z, Darnell JE, Jr (1994) Stat3: A STAT family member activated by tyrosine phosphorylation in response to epidermal growth factor and interleukin-6. *Science* 264:95–98.
84. Qian X, et al. (2008) In vivo tumor targeting and spectroscopic detection with surface-enhanced Raman nanoparticle tags. *Nat Biotechnol* 26:83–90.
85. El-Sayed IH, Huang X, El-Sayed MA (2005) Surface plasmon resonance scattering and absorption of anti-EGFR antibody conjugated gold nanoparticles in cancer diagnostics: Applications in oral cancer. *Nano Lett* 5:829–834.
86. Sadauskas E, et al. (2009) Protracted elimination of gold nanoparticles from mouse liver. *Nanomedicine (Lond)* 5:162–169.
87. Ali MR, et al. (2017) Efficacy, long-term toxicity, and mechanistic studies of gold nanorods photothermal therapy of cancer in xenograft mice. *Proc Natl Acad Sci USA* 114:E3110–E3118.
88. Ali MR, Ibrahim IM, Ali HR, Selim SA, El-Sayed MA (2016) Treatment of natural mammary gland tumors in canines and felines using gold nanorods-assisted plasmonic photothermal therapy to induce tumor apoptosis. *Int J Nanomedicine* 11: 4849–4863.
89. Galbraith CG, Yamada KM, Galbraith JA (2007) Polymerizing actin fibers position integrins primed to probe for adhesion sites. *Science* 315:992–995.
90. Mattila PK, Lappalainen P (2008) Filopodia: Molecular architecture and cellular functions. *Nat Rev Mol Cell Biol* 9:446–454.
91. Wu Y, et al. (2014) Five-plex isotope dimethyl labeling for quantitative proteomics. *Chem Commun (Camb)* 50:1708–1710.
92. Choudhary C, et al. (2009) Lysine acetylation targets protein complexes and co-regulates major cellular functions. *Science* 325:834–840.
93. Mecham BH, Nelson PS, Storey JD (2010) Supervised normalization of microarrays. *Bioinformatics* 26:1308–1315.